nature geoscience

SUPPLEMENTARY INFORMATION

DOI: 10.1038/NGEO1837

Intensification of open-ocean oxygen depletion by vertically migrating animals

Daniele Bianchi, Eric D. Galbraith, David A. Carozza, K.A.S. Mislan, Charles A. Stock

This pdf file includes:

Analysis of the ADCP and estimate of daytime DVM depths

We analyzed 1455 cruises from the US National Oceanic Data Center Joint Archive for Shipboard Acoustic Doppler Current Profilers (ADCPs) and from the British Oceanographic Data Center. We selected 389 cruises that showed at least one detectable DVM event in the ADCP echo intensity signal. Several cruises had to be excluded because they did not allow for the detection of DVM events, owing to a combination of reasons, including ADCP data (1) extending only few hundred meters deep, thus missing the lower parts of DVM events; (2) having too many temporal gaps; (3) being too noisy; (4) having a large proportion of "bad" flags.

To focus on DVM patterns that penetrated into the mesopelagic zone, we excluded migrations shallower than approximately 150-200 m. We excluded all data that were flagged as 'bad', and corrected echo intensities by subtracting the mean of the lowest 10% of the data from each profile to remove background noise.

For each detectable DVM event (4640 in total) we estimated the daytime DVM depth from: (1) the maximum subsurface day-to-night echo intensity difference, and (2) the maximum subsurface daytime backscatter. In the first case we calculated the difference in ADCP echo intensity averaged over a 3-hour interval centered at the time of maximum solar elevation (midday) and the ADCP echo intensity averaged over a 3-hour interval centered at the time of minimum solar elevation (midnight) for the nights surrounding the DVM event. We then detected the depth of the maximum subsurface echo intensity difference. In the second case, we estimated the depth of the midday subsurface backscatter maximum. Backscatter was estimated from the ADCP echo intensity by correcting for both sound-wave spherical attenuation and water absorption using the formulation of ref. [1]. The use of the two methods increased the number of records for which the daytime DVM depth could be isolated. Whenever both methods provided a valid daytime DVM depth, the average of the two values was taken.

Overall, the two methods produced similar results (Fig. S1). The estimated daytime DVM depths are the same (within a 8 m bin depth resolution) for 38 % of the events, and differ by less than 50 m for 80 % of the events. Only 7 % of the events showed depths differing by more than 100 m. Some acoustic profiles are characterized by multiple scattering layers with daytime DVM depths generally less than 100 m apart. In the cases where multiple migrating sound scattering layers were present, we isolated the layer that returned the strongest backscatter signal.

The gridded dataset shown in Fig. 2 was generated by averaging the daytime DVM depths in 4° by 4° areas. Fig. S2 and S3 show the number of measurements and standard deviations of the gridded data in each box.

Relationship between light and daytime DVM depths

We estimate the ability of water column light intensity to predict daytime DVM depths by calculating the peak irradiance in the water column from observed surface shortwave radiation, climatological profiles of chlorophyll [2], and chlorophyll-dependent light absorption [3,4].

We calculated the light levels and isolume depths at the time and locations of the DVM records by combining daytime surface shortwave radiation from the NOAA Climate Forecast System Reanalysis and chlorophyll-dependent light attenuation coefficients. Chlorophyll profiles were determined using the parameterization of ref.[2] forced with climatological surface chlorophyll from NASA Goddard Center SeaWiFS data, and climatological mixed layer depths[5]. We used the light attenuation scheme of ref. [3] for the full shortwave spectrum, and the light attenuation scheme of ref. [4] for selected shortwave bands in the 400-500 nm range, corresponding to the deepest light penetration in the ocean, and the maximum zooplankton and micronekton vision sensitivities[6].

According to the isolume hypothesis[7], DVM daytime depth should correspond to a small range of light intensities. However, the maximum light intensity over the visible spectrum at the daytime DVM depths varies between 10^{-7} and 10^{-2} W m^{-2} (mean Log_{10} of the irradiance in W m^{-2} of -4.0 ± 0.8, Fig. S4). This wide range of light intensities at the daytime DVM depths (Fig. S4) does not support the existence of a single global isolume determining the depth of migrations. However, it is possible that that light cues are modulated, worldwide, by additional environmental factors, or that distinct populations of migrating organisms respond differently to light stimuli, so that distinct isolumes control migrations in different oceanographic provinces.

At the global scale, the depth of the mean global isolume (10^{-4} W m^{-2}) shows a poor ability in predicting the daytime DVM depths ($R^2 = 0.20$, $p < 0.01$, Fig. S5). Although some of

the features of the daytime DVM depths are mirrored by global isolume depths, for example deepening towards the central subtropical gyres, and shallowing towards polar and upwelling regions, isolume depths underestimate the magnitude of DVM depth excursions between such regions. Vertical migrations tend to be deeper than the mean global isolume in the subtropical gyres and in the high latitude South Pacific, and shallower in the Indian Ocean, Eastern Tropical Pacific, and Subarctic Pacific. Similar results hold for wavelength-dependent global isolumes.

Regression between oceanographic property and DVM depth

We tested the ability of different oceanographic variables in predicting daytime DVM depths. Of all the variables considered, the largest significant correlations to daytime DVM depths were found for oxygen, chlorophyll and mixed layer depths. Shallower migrations where observed in regions characterized by lower subsurface oxygen, higher surface chlorophyll and shallower mixed layer depths. A stepwise multiple linear regression also included temperature as a significant predictor. We chose to use the differences between surface and mid-depth oxygen and temperature as predictors in order to represent the range of conditions that migrators experience throughout each DVM cycle. We obtained analogous results, with slightly smaller correlation coefficients, when we used the absolute values of oxygen and temperature instead of surface to mid-depth differences. We used climatological data to calculate the oxygen and temperature differences between 0 - 25 m and 150 - 500 m depth (ΔO_2, mmol m^{-3}, and ΔT, °C), the Log_{10} of surface chlorophyll (Chl, mg m^{-3}) and mixed layer depths (mld, m) at the months and locations of the DVM records. We used monthly climatological oxygen and temperature from the NODC World Ocean Atlas Dataset 2005; monthly climatological chlorophyll from

NASA Goddard Center SeaWiFS data, and monthly climatological mixed layer depths from ref. [5]. The resulting daytime DVM depth (m) from a stepwise multiple linear regression is:

$$Z_{DVM} = 398 - 0.56 \cdot \Delta O_2 - 115 \cdot Log_{10}(Chl) + 0.36 \cdot mld - 2.4 \cdot \Delta T$$

with the following 95 % confidence intervals for each term respectively: 391, 405; -0.59, -0.53; -121, -108; 0.31, 0.42; -2.7, -2.1. The root mean square error of the regression is 53 m.

Although more complex models can be designed, a linear regression showed to be sufficient to explain a large proportion of the DVM patterns ($R^2 = 0.60$, $p < 0.01$, Fig. S6). Similar results can be obtained using net primary production (NPP) or export production instead of chlorophyll. However, we chose to use chlorophyll alone because large-scale observational datasets of NPP and export production are based on empirical relationships that use satellite chlorophyll and temperature observations (e.g. Dunne et al., 2007 and references therein), and thus do not represent truly independent variables. Physical and biogeochemical properties vary in concert in the ocean and are not completely uncorrelated. However, within the uncertainty bounds, we obtained the same regression coefficients after linear regularization of the regression.

Diel vertical migrations and oxygen profiles

The global analysis in Fig. 1, and the results from the multiple linear regression analysis show shallow migrations in the major open ocean OMZs, to depths that correspond to hypoxic and suboxic concentrations, and deeper migrations in well oxygenated waters. Inspection of DVM depths in relation to oxygen profiles (Fig. S7) indicates that in regions where oxygen minima are present, migrators reach well within the hypoxic (O_2<60 mmol m^{-3}) and, where present, suboxic (O2<5 mmol m^{-3}) domains, often spending the daytime in proximity of the core of the OMZ, as

in the case of the shallower South Eastern Tropical Pacific, North Eastern Tropical Atlantic, South Eastern Tropical Atlantic, and Bay of Bengal oxygen minima. This association between DVM and oxygen minima supports and extend previous local surveys[8-10], and is consistent with the hypothesis that hypoxic and suboxic waters might provide a refuge from large predators with high oxygen requirements[11,12].

Ocean Circulation-Biogeochemistry Model

The model used in this study is the 3-degree resolution GFDL MOM4p1 ocean model coupled with the BLINGv0 biogeochemistry model[13]. MOM4p1 is a pressure coordinate, free-surface ocean model that includes parameterizations of mesoscale and sub-submesoscale processes and mixed layer dynamics. The model is forced with heat, freshwater and shortwave fluxes from climatologies. BLING is a computationally efficient biogeochemical model consisting of four explicit tracers (dissolved inorganic and organic phosphorous, iron and oxygen) with a representation of macronutrient, micronutrient, and light limitation, and an implicit treatment of ecosystem community structure. Organic matter production by photosynthesis is partitioned between an explicit dissolved pool and implicit sinking particle and DVM fluxes.

We assume that DVM fluxes are a constant fraction of the organic matter export production, and we vary this fraction between 0 and 0.45, spanning the range of existing observational and model estimates listed in the Supplementary Table S1.

Particle respiration that is not associated with DVM follows a typical observationally-based power law profile[14]. DVM active transport is returned to the water column via a migratory respiration flux, assumed to be uniform between the surface and the daytime DVM depth, and a deep respiration flux shaped as a Gaussian, centered at the daytime DVM depth, with a scale

parameter of 50 m, in agreement with observations[9,15] and previous modeling studies[16]. The partitioning between migratory and deep respiration fractions is scaled according to the duration of migrations, assumed to be proportional to the local DVM depth. The DVM depth is determined in the model using the multiple linear regression equation and is shown in Fig. S8. This redistribution presumes that the respiration associated with organic material consumed near the surface continues throughout the day. To simulate the lack of diurnal migrations in the wintertime high latitudes, the DVM depth is linearly decreased to 150 m when the daily mean surface irradiance decreases below 10 W m^{-2}. Oxygen consumption by respiration is calculated from the phosphate remineralization rate using a stoichiometric ratio of 150:1, and is set to zero at oxygen concentrations below 1.0 mmol m^{-3}. The profiles of respiration due to the active DVM transport and to the remineralization of passive detritus are shown in Fig. S9 for DVM export fractions equal to 0.15, 0.30 and 0.45. The models were integrated for 1500 years until approximate equilibrium was reached, and the last 100 years of simulations were analyzed.

In the models, the oxygen utilization due to migrators shows an approximately linear dependency with the active export fraction at any given location (Fig. S10). That means that, for example, a doubling of the active export fraction results in a doubling of the oxygen consumption due to vertically migrating organisms. This result allows us to use the different model runs to calculate the slope between the active export fraction and the oxygen utilization due to DVM and express it in units of mmol m^{-3} per each % of export by DVM relative to particle export, as shown in Fig 3. We note that a mechanistic model of migrator biomass, together with specific respiration rates, could be used to quantify the impact of animal respiration on oxygen instead of adopting a fixed DVM export fraction. This would require a predictive model of zooplankton and micronekton

biomass, and of the proportion of migrators. While global models have only recently started to simulate animal biomass adequately, a predictive framework for the fraction of migrators is still lacking. The theoretical and observational uncertainties surrounding the migrating fraction and the DVM export persuaded us to express the oxygen utilization due to DVM as a function of the active export fraction (Fig. 3). Together with the range of active export fractions reviewed in Table S1, this can be directly used to estimate the effects of migrations on water column chemistry and oxygen distribution in a general sense.

Supplementary Table S1. Observational and model-based estimates of active organic matter export relative to particle export (DVM/POC export, percent).

Location	DVM/POC export (%)	Reference
Median of 9 oceanic sites(1)	26	17
North Atlantic (NFLUX) (2)	8	18
Eastern Tropical Pacific (2 sites) (3)	25-45	19
Subtropical North Atlantic and North Atlantic (5 sites) (3)	14-53	19
Subtropical North Atlantic (BATS) (4)	34 (18-70)	20
Equatorial Pacific (EqPac) (5)	31-44	21
North Atlantic (NABE) (6)	19-40	22
Subtropical North Atlantic (BATS) (7)	8 (0-39)	23
Subtropical North Pacific (ALOHA) (8)	15	24
Western Equatorial Pacific (9)	30-48 (uncorrected) 50-100 (corrected)	25
Subtropical North Atlantic (Canary Islands) (10)	25 (16-45)	26
Subtropical North Atlantic (Canary Islands) (11)	15-53	27
Subtropical North Pacific (12)	20	28
Subtropical North Atlantic (BATS) (13)	15	29
North Pacific Ocean (subpolar to equatorial) (14)	15-40	16

(1) Longhurst and Harrison (1988) (ref. [17]). Biomass data for migratory zooplankton and micronekton from 9 stratified low-latitude sites are used in conjunction with estimates of excretion rates to calculate the DVM active transport. Primary production data are used to estimate the particle flux at 100 m depth.

(2) Longhurst et al. (1989) (ref. [18]). NFLUX station (38N, 65W). Export fluxes out of the euphotic zone (100-120 m). DVM active transport estimated from $NH4^+$ excretion rates; particle flux from sediment trap data.

(3) Longhurst et al. (1990) (ref. [19]). Export fluxes across the upper ocean density discontinuity (47-100 m in the Eastern Tropical Pacific; 58-200 m in the Subtropical Atlantic). DVM active transport estimated from migratory mesozooplankton and micronekton biomass together with estimates of excretion rates from the literature; particle flux is calculated from primary production measurements.

(4) Dam et al. (1995) (ref. [20]). JGOFS BATS station (31N, 64W). DVM export fluxes at 150 m depth from daytime and nighttime mesozooplankton biomass measurements combined with published metabolic rates. Particle fluxes at 150 m depth from sediment traps.

(5) Zhang and Dam (1997) (ref. [21]). JGOFS EqPac station (0N,140W). DVM export fluxes from the euphotic zone estimated from daytime and nighttime mesozooplankton biomass measurements combined with published metabolic rates. Particle fluxes from the euphotic zone from sediment traps.

(6) Morales (1999) (ref. [22]). JGOFS NABE cruises (3 cruises between 41N-63N and 14W-18W). DVM (mesozooplankton) and particle export fluxes out of the surface layers (100 m depth) from literature and JGOFS-NABE data in the North Atlantic.

(7) Steinberg et al. (2000) (ref. [23]). JGOFS BATS site (31N, 64W). DVM export fluxes at 150 m depth from daytime and nighttime mesozooplankton biomass measurements combined with metabolic rate estimates from the literature. Particle fluxes at 150 m depth from sediment traps.

(8) Al-Mutahiri and Landry (2001) (ref. [24]). Station ALOHA (22N, 158W). DVM export fluxes at 155 m depth from daytime and nighttime mesozooplankton biomass measurements combined with metabolic rate estimates from the literature. Particle fluxes at 150 m depth from sediment traps.

(9) Hidaka et al. (2001) (ref. [25]). Western equatorial Pacific (3N-145W). DVM export fluxes at 160 m depth from daytime and nighttime mesozooplankton and micronekton biomass measurements combined with metabolic rate estimates from the literature. Particle fluxes at 160 m depth from sediment traps. The corrected values include an upward estimate of the migratory micronekton biomass obtained by assuming a 14 % micronekton sampling effciency of the trawls.

(10) Hernandez Leon et al. (2001) (ref. [26]). Canary Islands. DVM export fluxes at 200 m depth from daytime and nighttime mesozooplankton biomass measurements combined with in situ metabolic rate measurements. Particle fluxes at 150 m depth from literature data.

(11) Yebra et al. (2005) (ref. [27]). For methods, see (10).

(12) Hannides et al. (2009) (ref. [28]). Station ALOHA (22N, 158W). DVM export fluxes at 160 m depth from daytime and nighttime mesozooplankton biomass measurements combined with metabolic rate estimates from the literature. Particle fluxes at 150 m depth from sediment traps.

(13)Steinberg et al., (2012) (ref. [29]). 17-year timeseries at the JGOFS BATS site (31N, 64W). DVM export fluxes at 150 m depth from daytime and nighttime mesozooplankton biomass measurements combined with metabolic rate estimates from the literature. Particle fluxes at 150 m depth from sediment traps.

(14) Bianchi et al. (in press) (ref.[16]). Modelling study based on a 1-D multiple size-class NPZD model which includes explicit representation of DVM dynamics, calibrated against observed productivity and biomasses for three sites in the Pacific Ocean.

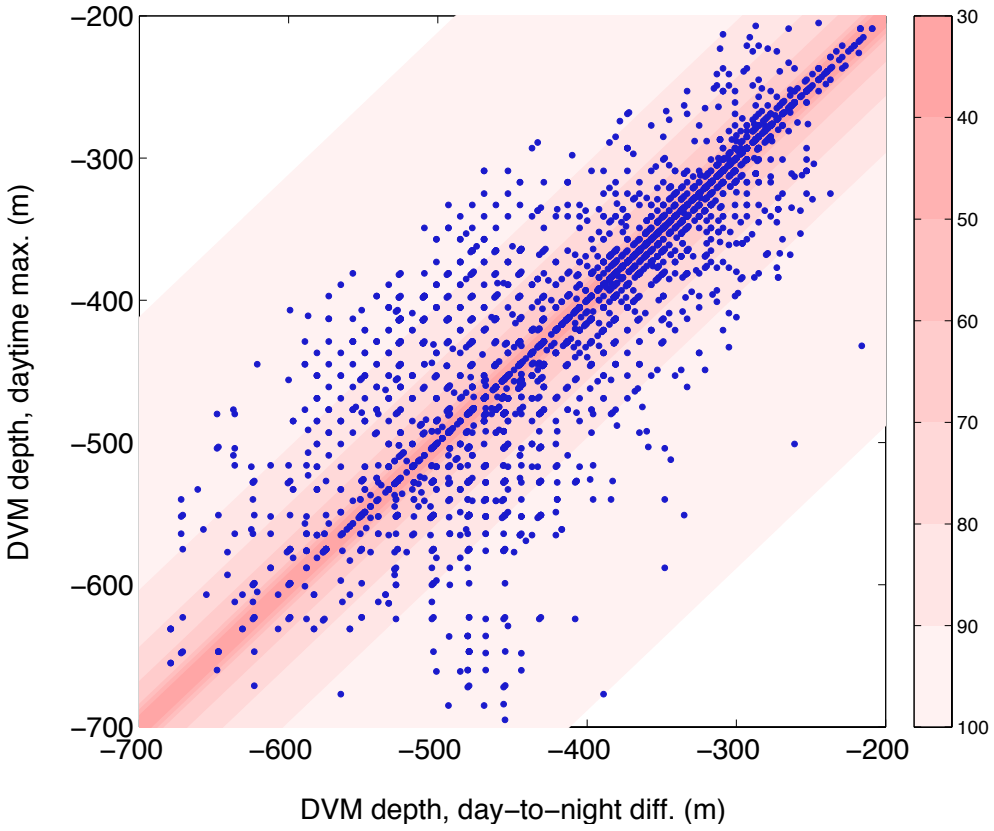

Figure S1. Relationship between different estimates of DVM depth. The figure shows a scatter plot of the DVM depth from daytime maximum subsurface backscatter versus DVM depth from day-to-night ADCP amplitude difference. The colour shading shows the density distribution of the data (percent). 30 % of the data show identical depths; 80 % of the data show differences less than 50 m.

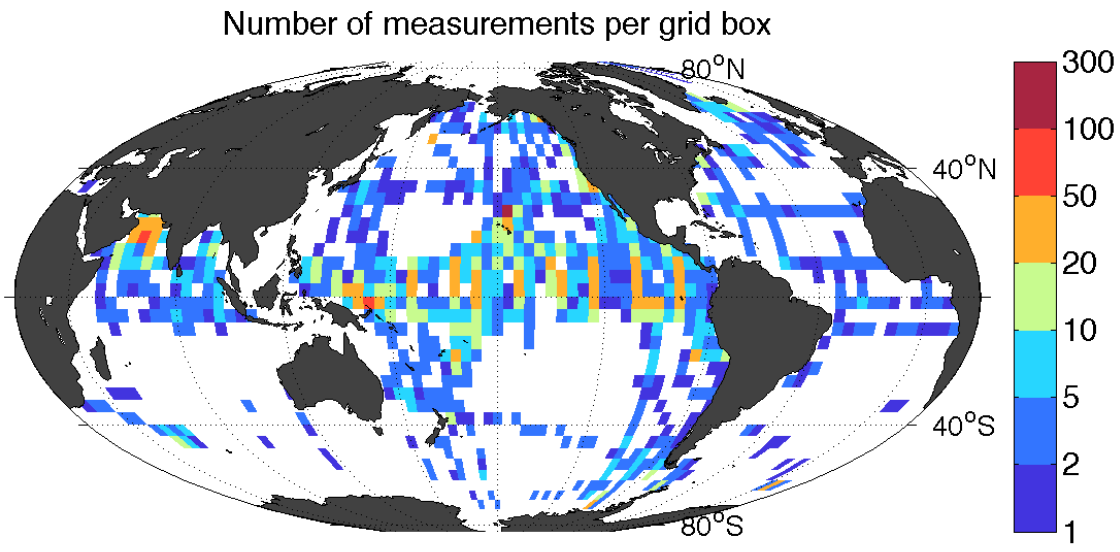

Figure S2. **Number of DVM depth observations.** The figure shows the number of DVM events detected in the ADCP data for each of the 4° by 4° areas used to generate Fig. 2.

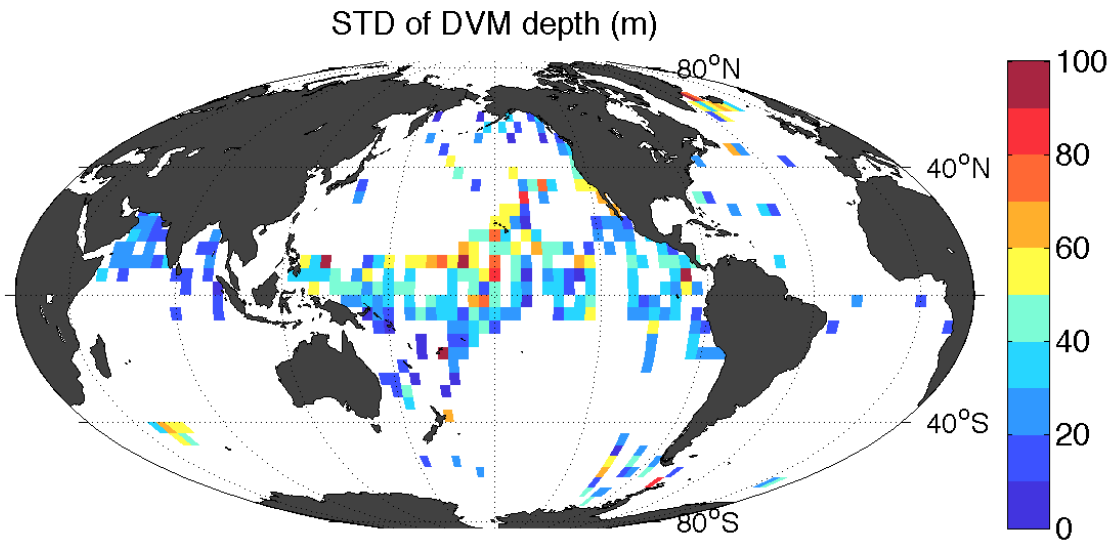

Figure S3. **Standard deviations of DVM depths.** The figure shows the standard deviation of the DVM depths for each of the 4° by 4° areas shown in Fig. 2. Values are shown only for grid areas containing 3 DVM depth estimates or more.

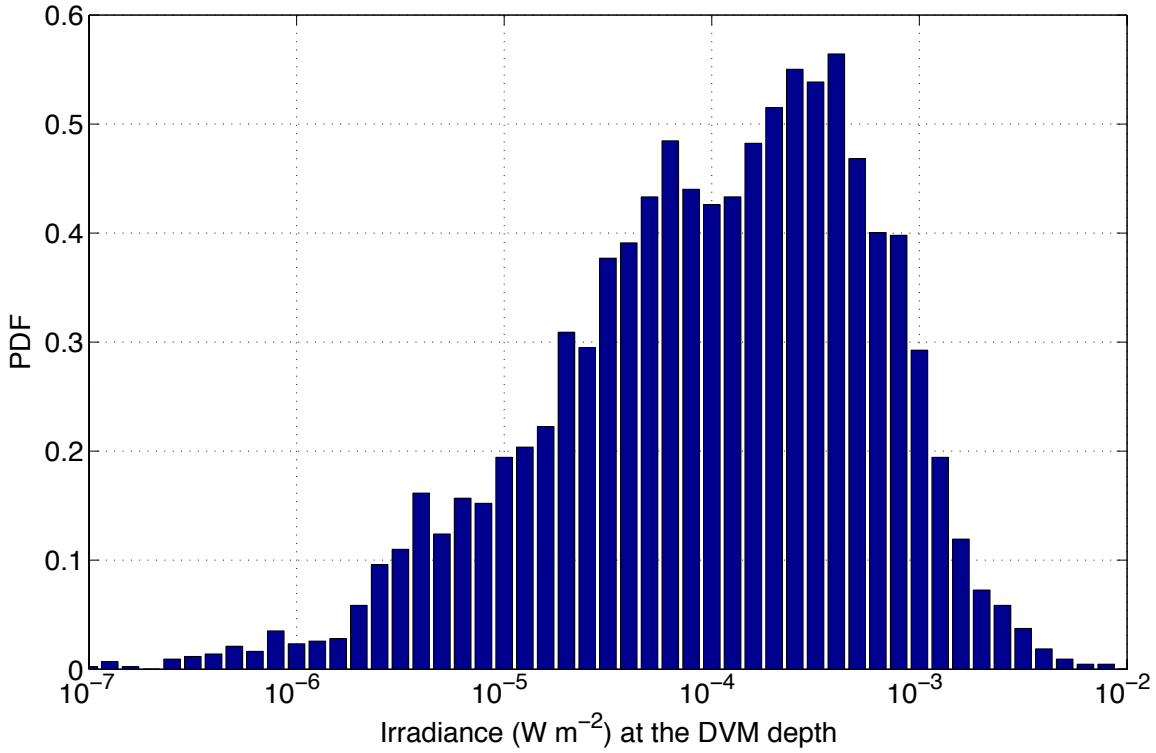

Figure S4. **Probability distribution function of the irradiance (W m^{-2}) at the daytime DVM depth.** The probability distribution was calculated by dividing the number of measurements in each irradiance bin by the bin width. The irradiance was estimated using the light penetration scheme of ref. [3] using surface irradiance and depth-dependent chlorophyll from climatologies.

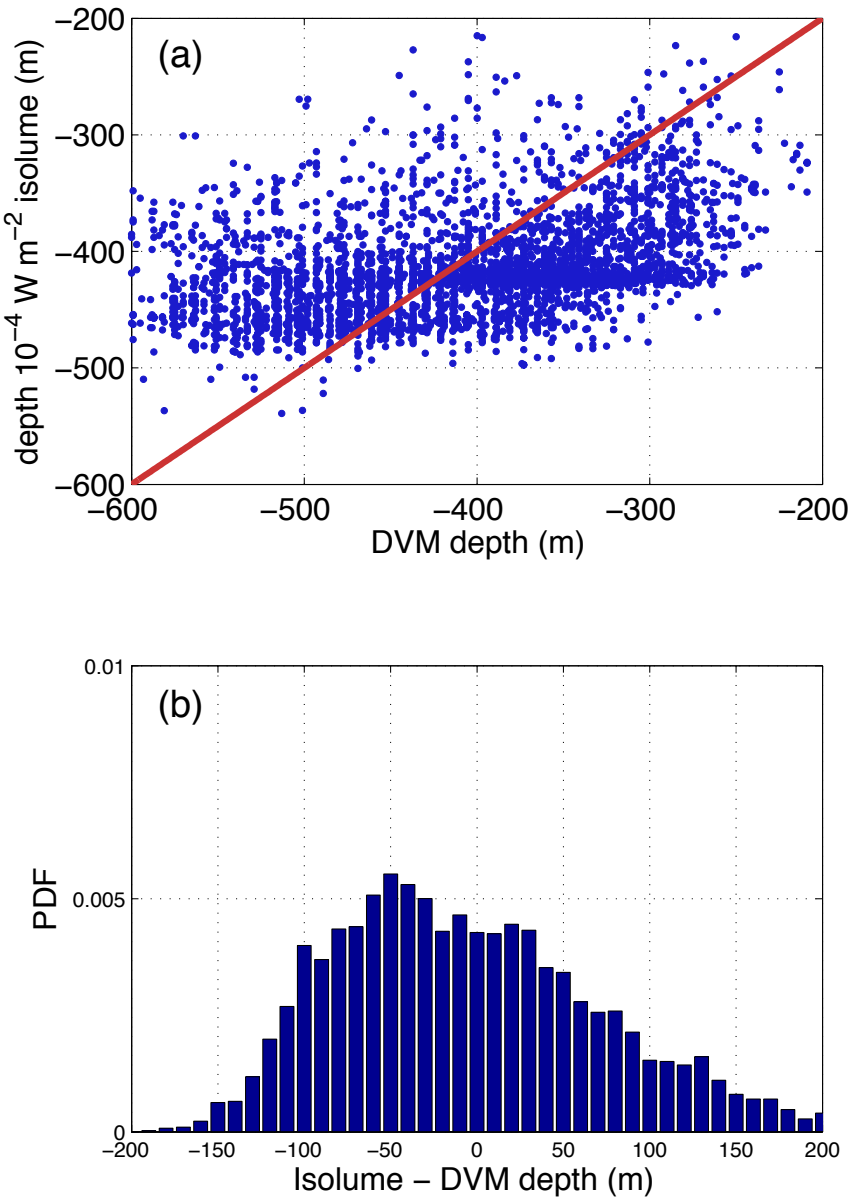

Figure S5. Daytime DVM depth predicted from global isolume depth. (**A**) Scatter plot of the depth of the mean isolume (10^{-4} Wm^{-2}) versus the DVM depth. The correlation coefficient is $R^2 = 0.20$ ($p < 0.01$). The red line is the 1:1 line. (**B**) Probability distribution function of the difference between isolume depth and daytime DVM depth. The probability distribution was calculated by dividing the number of measurements in each depth bin by the bin width. The mean and standard deviation of the distribution are 0 and 80 m respectively.

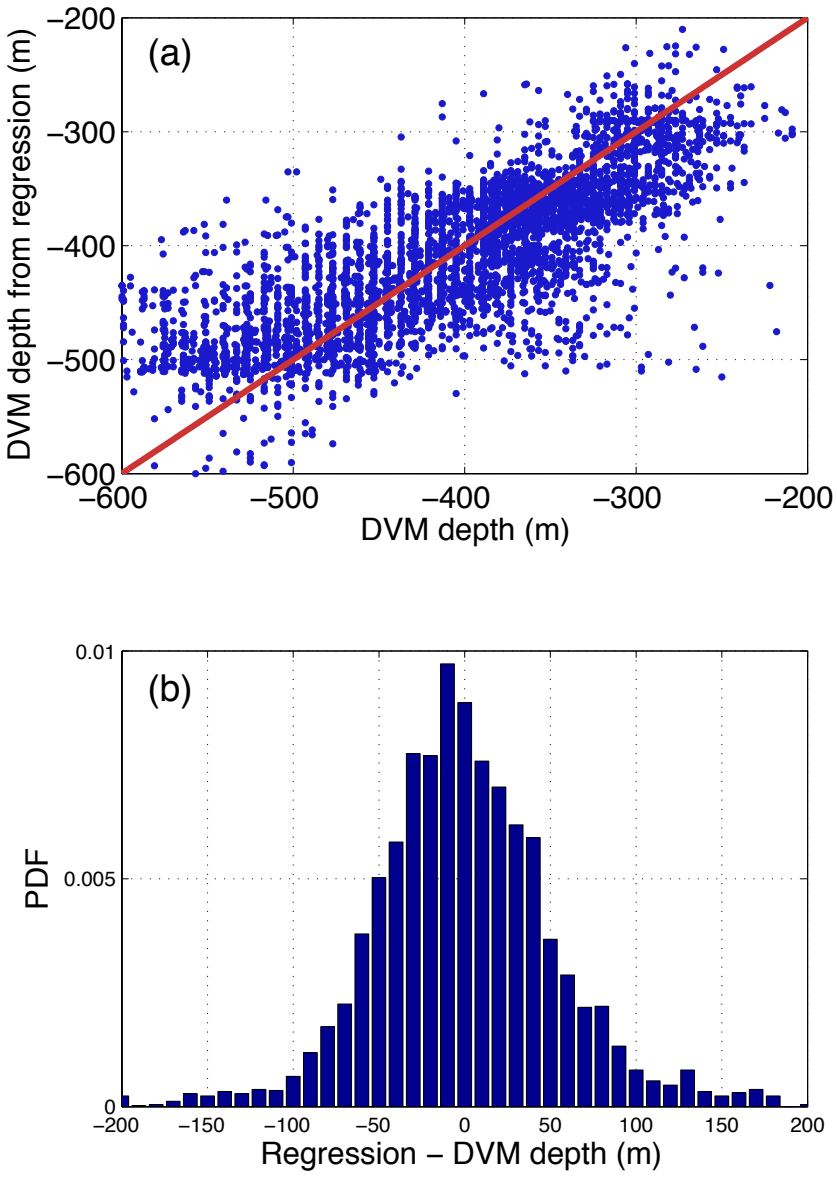

Figure S6. Daytime DVM depth predicted from environmental variables. (**A**) Scatter plot of the DVM depth estimated from a stepwise multiple linear regression versus the actual DVM depth. The coefficient of determination of the regression is $R^2 = 0.60$ ($p < 0.01$). The red line is the 1:1 line. (**B**) Probability distribution function of the difference between daytime DVM depth from the regression and observed daytime DVM depth. The probability distribution was calculated by dividing the number of measurements in each depth bin by the bin width. The mean and standard deviation of the distribution are 0 and 54 m respectively.

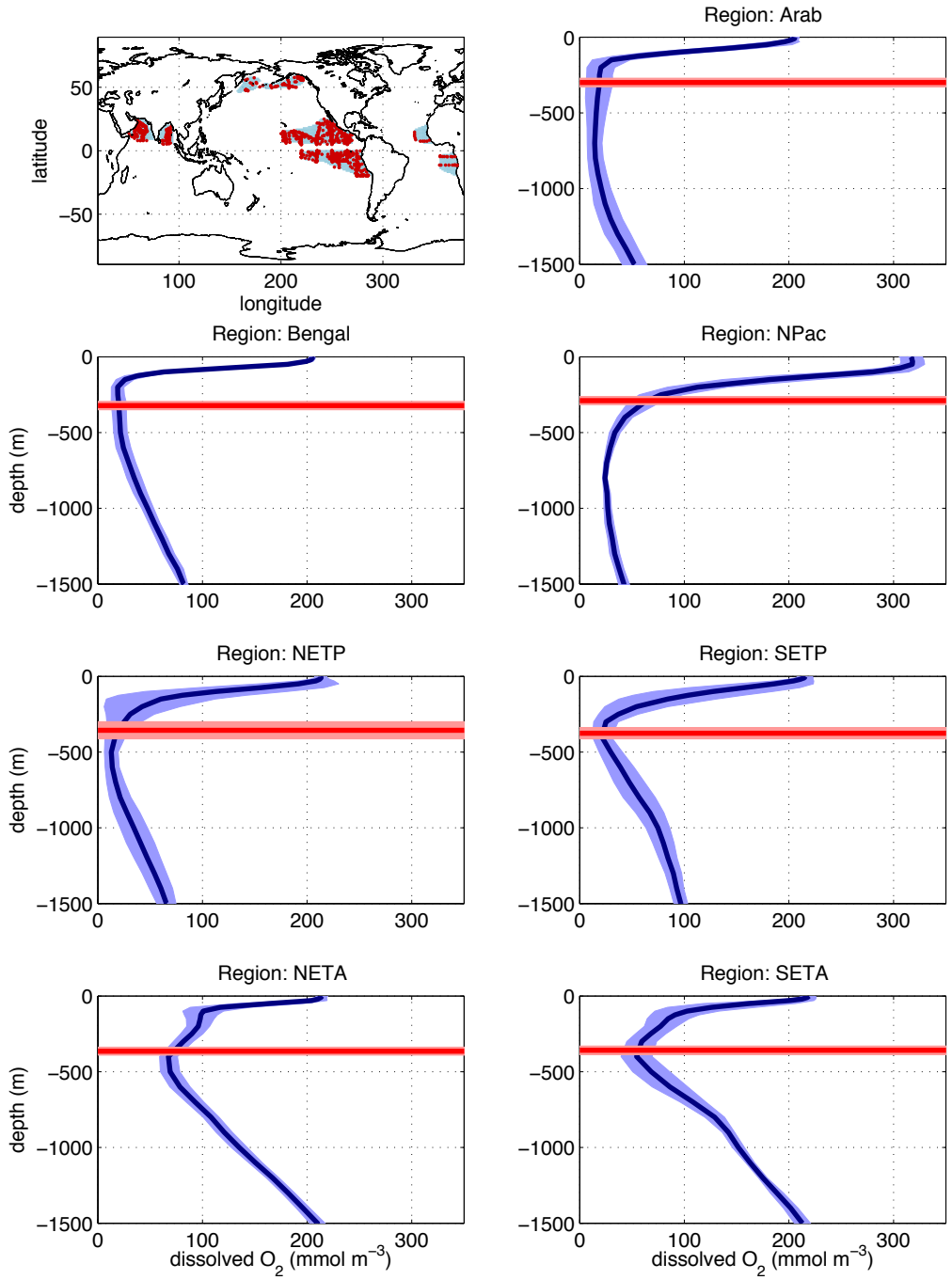

Figure S7. **Relationship between daytime DVM depths and oxygen profiles.** The first panel shows a map of the 7 major open ocean oxygen minimum zones (blue shading) and the locations of single DVM events detected in the acoustic data within each of the regions (red dots.) The following panels show in blue the average oxygen profiles (mmol m^{-3}) from each region from the

World Ocean Atlas, and in red the location of the average DVM depth detected in the acoustic data. Shadings show one standard deviation around the means. The regions are: Arabian Sea, Bay of Bengal, North Pacific, North Eastern Tropical Pacific, South Eastern Tropical Pacific, North Eastern Tropical Atlantic, South Eastern Tropical Atlantic.

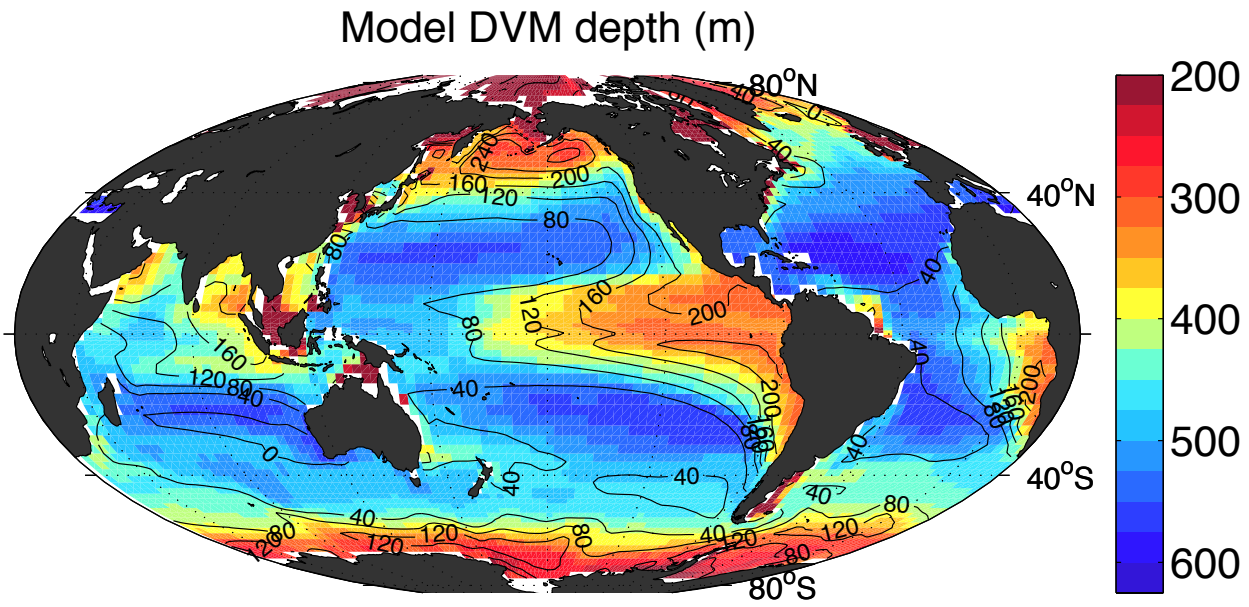

Figure S8. **Annual mean DVM depth (m) in the model.** Daytime DVM depths (colours) predicted using the regression of equation S1, using model temperature, oxygen, chlorophyll and mixed layer depths. Contours show the surface (0 - 25 m) to upper mesopelagic zone (150 - 500 m) oxygen difference (mmol m^{-3}).

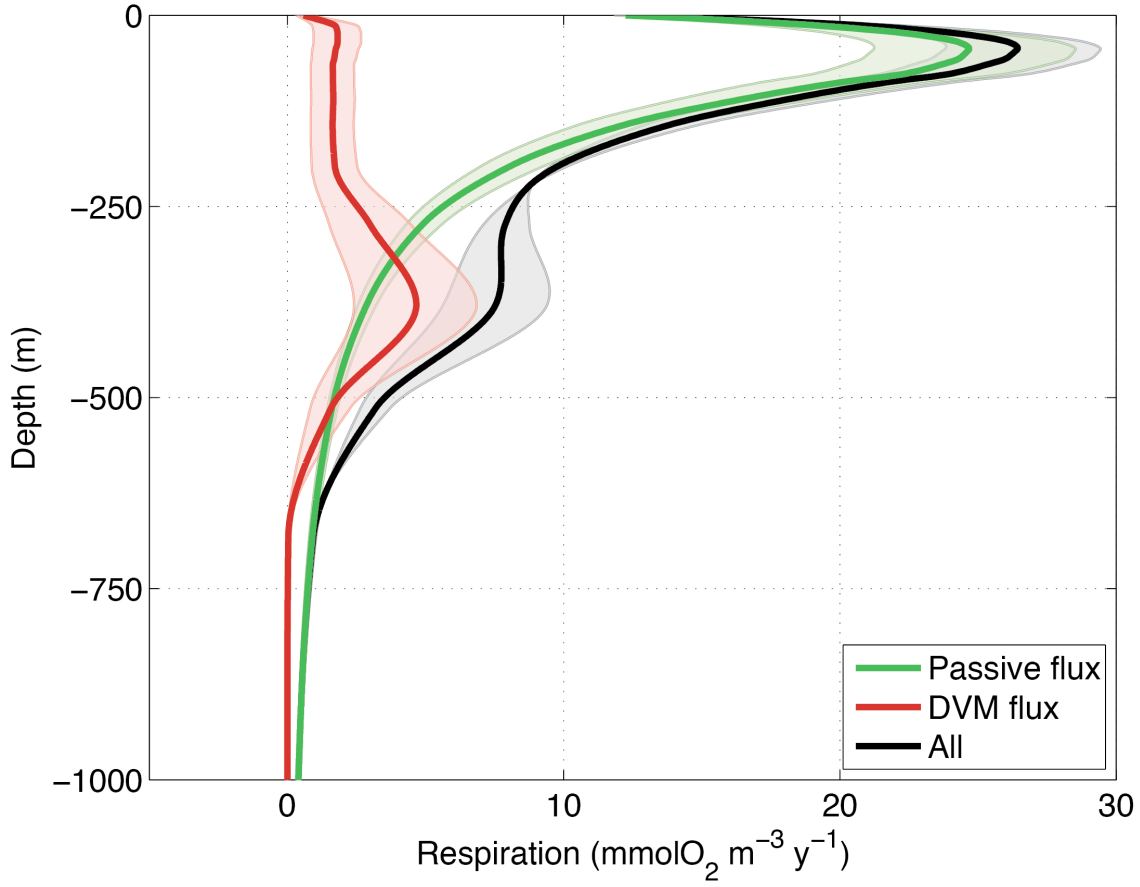

Figure S9. **Globally averaged respiration (mmol m^{-3} $year^{-1}$) in the model**. The green line shows the passive detritus respiration (sinking particles and dissolved organic matter), the red line shows the respiration due to active DVM transport, and the black line the sum of the two. Results are shown for active DVM flux equal to 0.3 times the organic matter export production. The light-coloured shadings indicate the envelope values obtained with active DVM fractions equal to 0.15 and 0.45 times the organic matter export production respectively.

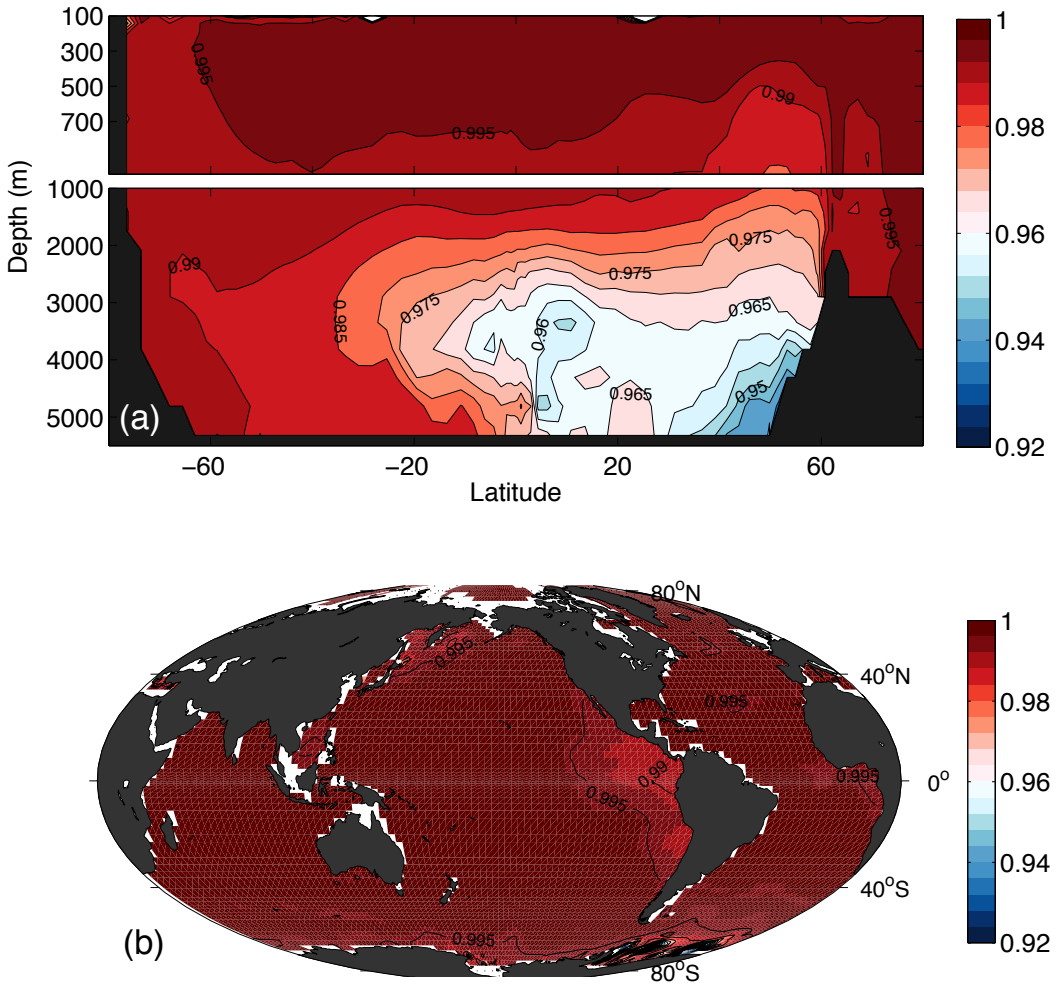

Figure S10. **Correlation between the active export fraction and the oxygen utilization due to DVM in the model**. The correlation coefficients were calculated at each model grid point, using the oxygen utilization due to DVM from 4 model runs where the active export fraction was varied between 0 and 0.45. (A) Zonal average. Values shallower than 100 m were excluded because approaching the surface oxygen utilizations tend to zero resulting in noisy correlations. Lower correlation in the abyssal ocean might be due to incomplete model equilibration after the 1500 year spin up. (B) Average over the upper mesopelagic zone (150 - 500 m).

Supplementary References

1 Deines, K. L. Backscatter estimation using broadband acoustic Doppler Current Profilers. *Proceedings of the Ieee Sixth Working Conference on Current Measurement*, 249-253 (1999).

2 Uitz, J., Claustre, H., Morel, A. & Hooker, S. B. Vertical distribution of phytoplankton communities in open ocean: An assessment based on surface chlorophyll. *J Geophys Res-Oceans* **111** (2006).

3 Manizza, M., Le Quere, C., Watson, A. J. & Buitenhuis, E. T. Bio-optical feedbacks among phytoplankton, upper ocean physics and sea-ice in a global model. *Geophys Res Lett* **32** (2005).

4 Morel, A. & Maritorena, S. Bio-optical properties of oceanic waters: A reappraisal. *J Geophys Res-Oceans* **106**, 7163-7180 (2001).

5 Montegut, C. D., Madec, G., Fischer, A. S., Lazar, A. & Iudicone, D. Mixed layer depth over the global ocean: An examination of profile data and a profile-based climatology. *J Geophys Res-Oceans* **109** (2004).

6 Warrant, E. J. & Locket, N. A. Vision in the deep sea. *Biol Rev* **79**, 671-712 (2004).

7 Cohen, J. H. & Forward, R. B. Zooplankton Diel Vertical Migration - a Review of Proximate Control. *Oceanogr Mar Biol* **47**, 77-109 (2009).

8 Barham, E. G. Deep Scattering Layer Migration and Composition - Observations from a Diving Saucer. *Science* **151**, 1399-& (1966).

9 Luo, J. G., Ortner, P. B., Forcucci, D. & Cummings, S. R. Diel vertical migration of zooplankton and mesopelagic fish in the Arabian Sea. *Deep-Sea Res Pt Ii* **47**, 1451-1473 (2000).

10 Ashjian, C. J., Smith, S. L., Flagg, C. N. & Idrisi, N. Distribution, annual cycle, and vertical migration of acoustically derived biomass in the Arabian Sea during 1994-1995. *Deep-Sea Res Pt Ii* **49**, 2377-2402 (2002).

11 Seibel, B. A. Critical oxygen levels and metabolic suppression in oceanic oxygen minimum zones. *J Exp Biol* **214**, 326-336 (2011).

12 Stramma, L. *et al.* Expansion of oxygen minimum zones may reduce available habitat for tropical pelagic fishes. *Nat Clim Change* **2**, 33-37 (2012).

13 Galbraith, E. D., Gnanadesikan, A., Dunne, J. P. & Hiscock, M. R. Regional impacts of iron-light colimitation in a global biogeochemical model. *Biogeosciences* **7**, 1043-1064 (2010).

14 Martin, J. H., Knauer, G. A., Karl, D. M. & Broenkow, W. W. Vertex - Carbon Cycling in the Northeast Pacific. *Deep-Sea Research Part a-Oceanographic Research Papers* **34**, 267-285 (1987).

15 Steinberg, D. K., Cope, J. S., Wilson, S. E. & Kobari, T. A comparison of mesopelagic mesozooplankton community structure in the subtropical and subarctic North Pacific Ocean. *Deep-Sea Res Pt Ii* **55** (2008).

16 Bianchi, D., Stock, C., Galbraith, E. D. & Sarmiento, J. L. Diel vertical migration: ecological controls and impacts on the biological pump in a one-dimensional ocean model. *Global Biogeochemical Cycles, in press* (2013).

17 Longhurst, A. R. & Harrison, W. G. Vertical Nitrogen Flux from the Oceanic Photic Zone by Diel Migrant Zooplankton and Nekton. *Deep-Sea Research Part a-Oceanographic Research Papers* **35**, 881-889 (1988).
18 Longhurst, A. R. *et al.* Nflux - a Test of Vertical Nitrogen Flux by Diel Migrant Biota. *Deep-Sea Res* **36**, 1705-1719 (1989).
19 Longhurst, A. R., Bedo, A. W., Harrison, W. G., Head, E. J. H. & Sameoto, D. D. Vertical Flux of Respiratory Carbon by Oceanic Diel Migrant Biota. *Deep-Sea Research Part a-Oceanographic Research Papers* **37**, 685-694 (1990).
20 Dam, H. G., Roman, M. R. & Youngbluth, M. J. Downward Export of Respiratory Carbon and Dissolved Inorganic Nitrogen by Diel-Migrant Mesozooplankton at the Jgofs Bermuda Time-Series Station. *Deep-Sea Res Pt I* **42**, 1187-1197 (1995).
21 Zhang, X. S. & Dam, H. G. Downward export of carbon by diel migrant mesozooplankton in the central equatorial Pacific. *Deep-Sea Res Pt Ii* **44**, 2191-2202 (1997).
22 Morales, C. E. Carbon and nitrogen fluxes in the oceans: the contribution by zooplankton migrants to active transport in the North Atlantic during the Joint Global Ocean Flux Study. *J Plankton Res* **21**, 1799-1808 (1999).
23 Steinberg, D. K. *et al.* Zooplankton vertical migration and the active transport of dissolved organic and inorganic carbon in the Sargasso Sea. *Deep-Sea Res Pt I* **47**, 137-158 (2000).
24 Al-Mutairi, H. & Landry, M. R. Active export of carbon and nitrogen at Station ALOHA by diel migrant zooplankton. *Deep-Sea Res Pt Ii* **48**, 2083-2103 (2001).
25 Hidaka, K., Kawaguchi, K., Murakami, M. & Takahashi, M. Downward transport of organic carbon by diel migratory micronekton in the western equatorial Pacific: its quantitative and qualitative importance. *Deep-Sea Res Pt I* **48**, 1923-1939 (2001).
26 Hernandez-Leon, S. *et al.* Vertical distribution of zooplankton in Canary Island waters: implications for export flux. *Deep-Sea Res* **48**, 1071-1092 (2001).
27 Yebra, L., Almeida, C. & Hernandez-Leon, S. Vertical distribution of zooplankton and active flux across an anticyclonic eddy in the Canary Island waters. *Deep-Sea Res Pt I* **52**, 69-83 (2005).
28 Hannides, C. C. S. *et al.* Export stoichiometry and migrant-mediated flux of phosphorus in the North Pacific Subtropical Gyre. *Deep-Sea Res Pt I* **56**, 73-88 (2009).
29 Steinberg, D. K., Lomas, M. W. & Cope, J. S. Long-term increase in mesozooplankton biomass in the Sargasso Sea: Linkage to climate and implications for food web dynamics and biogeochemical cycling. *Global Biogeochem Cy* **26** (2012).